European Journal of Radiology 82 (2013) e87–e94

Contents lists available at SciVerse ScienceDirect

European Journal of Radiology

journal homepage: www.elsevier.com/locate/ejrad

Automatic multi-modal MR tissue classification for the assessment of response to bevacizumab in patients with glioblastoma

Gilad Liberman[a,b], Yoram Louzoun[c], Orna Aizenstein[a], Deborah T. Blumenthal[d], Felix Bokstein[d], Mika Palmon[a], Benjamin W. Corn[e], Dafna Ben Bashat[a,*]

[a] The Functional Brain Center, The Wohl Institute for Advanced Imaging, Tel Aviv Sourasky Medical Center, Tel Aviv, Israel
[b] Gonda Multidisciplinary Brain Research Center, Bar Ilan University, Ramat-Gan, Israel
[c] Mathematics Department, Bar-Ilan University, Ramat-Gan, Israel
[d] Neuro-Oncology Service, Tel Aviv Sourasky Medical Center, Tel Aviv, Israel
[e] Institute of Radiotherapy, Tel Aviv Sourasky Medical Center, Tel Aviv, Israel

ARTICLE INFO

Article history:
Received 14 June 2012
Received in revised form 30 August 2012
Accepted 3 September 2012

Keywords:
MRI
Automatic classification
Glioblastoma
Anti-angiogenic treatment

ABSTRACT

Background: Current methods for evaluation of treatment response in glioblastoma are inaccurate, limited and time-consuming. This study aimed to develop a multi-modal MRI automatic classification method to improve accuracy and efficiency of treatment response assessment in patients with recurrent glioblastoma (GB).

Materials and methods: A modification of the *k*-Nearest-Neighbors (*k*NN) classification method was developed and applied to 59 longitudinal MR data sets of 13 patients with recurrent GB undergoing bevacizumab (anti-angiogenic) therapy. Changes in the enhancing tumor volume were assessed using the proposed method and compared with Macdonald's criteria and with manual volumetric measurements. The edema-like area was further subclassified into peri- and non-peri-tumoral edema, using both the *k*NN method and an unsupervised method, to monitor longitudinal changes.

Results: Automatic classification using the modified *k*NN method was applicable in all scans, even when the tumors were infiltrative with unclear borders. The enhancing tumor volume obtained using the automatic method was highly correlated with manual measurements ($N = 33$, $r = 0.96$, $p < 0.0001$), while standard radiographic assessment based on Macdonald's criteria matched manual delineation and automatic results in only 68% of cases. A graded pattern of tumor infiltration within the edema-like area was revealed by both automatic methods, showing high agreement. All classification results were confirmed by a senior neuro-radiologist and validated using MR spectroscopy.

Conclusion: This study emphasizes the important role of automatic tools based on a multi-modal view of the tissue in monitoring therapy response in patients with high grade gliomas specifically under anti-angiogenic therapy.

1. Introduction

Glioblastoma (GB) is a grade IV tumor according to the WHO classification and is the most common and aggressive type of human primary brain tumor, constituting approximately 12–15% of all primary central nervous system (CNS) tumors. Recently, bevacizumab, a monoclonal antibody to vascular endothelial growth factor, has been approved by the FDA for use in patients with recurrent GB who have failed to respond to previous therapies. This treatment alone or in combination with cytotoxic agents achieved a relatively high response rate and significantly prolonged the median overall survival [1].

Evaluation of the efficacy of therapeutic agents in the treatment of recurrent malignant gliomas still relies in most clinical trials on traditional Macdonald's criteria [2]. This method uses volumetric estimation based on bi-dimensional measurements, according to the WHO standard for reporting results of cancer treatment, to enable a gross evaluation of the change in the enhancing region of the tumor [3,4]. However, tumors treated with antiangiogenic agents may display different patterns of infiltration, largely non-enhancing, highlighting the limitations of Macdonald's criteria [1,3,4] and requiring a multi-modal view of the tissue for clinical assessment. Recently, efforts have been made in neuro-oncology to revise Macdonald's criteria by including changes in hyperintense signal on FLAIR images to assess therapy response. Yet, volumetric measurements of the enhancing tumor are not always accurate and

* Corresponding author at: The Functional Brain Center, The Wohl Institute for Advanced Imaging, Tel Aviv Sourasky Medical Center, 6 Weizman Street, Tel Aviv 64239, Israel. Tel.: +972 3 6973953; mobile: +972 52 4262515; fax: +972 3 6973080.
E-mail address: dafnab@tlvmc.gov.il (D. Ben Bashat).

0720-048X/$ – see front matter © 2012 Elsevier Ireland Ltd. All rights reserved.
http://dx.doi.org/10.1016/j.ejrad.2012.09.001

hyperintense signal on FLAIR images may be ambiguous due to the tumor's infiltrative nature that limits its accurate measurement.

Tools for automatic image analysis based on multi-modal imaging can provide objective information about the tissue. These tools include supervised methods that require prior knowledge, usually given as a training set (a set of manually labeled tissues), and unsupervised algorithms which are data-driven, providing unidentified clusters that inherently differ, but whose significance must be further defined. Automatic tools have been previously used for volumetric measurements and brain tissue segmentation in various brain pathologies [5–7] including glioblastoma (GB) [8–10], and for creating recurrence probability maps [11]. However, variability in scanning protocols, acquisition parameters and patient movements, which are inherent in clinical settings, result in variable and incomplete data sets (i.e. missing values) that limit the use of such methods.

Given the limitations inherent in currently used methods, in this study, a fully automatic method based on a modification of the *k*-Nearest-Neighbors (*k*NN) algorithm [12] method was developed and applied to a multi-modal MRI data set with the aim of improving accuracy in assessment of therapy response to bevacizumab in patients with recurrent GB. By including missing values in the *k*NN algorithm, arising from substandard acquisitions or movements, and by performing voxel based classification based solely on MR characteristics rather than spatial/morphologic properties, this method aims to overcome the constraints of existing methods. Classification results were validated using manual labeling of the different tissue classes, MR spectroscopy (MRS), volumetric measurements of the enhanced tumor class using manual delineations and independent unsupervised classification algorithm. Therapy response assessment was performed based on the *k*NN results, Macdonald's criteria, and manual delineation of the enhancing tumor.

2. Materials and methods

2.1. Patients

A total of 59 MR scans from 13 patients with biopsy-confirmed GB (8 women, 5 men, mean age 52 ± 15 years, age range of 26–74 years) were acquired and analyzed. Patients were repeatedly scanned 3–11 times, at several time points before and during the therapy. All patients received bevacizumab as a second-line therapy, having previously undergone treatments including surgery, radiation and chemotherapies. Patients' clinical data are presented in Table 1. The study was approved by the hospital's institutional review board, and written informed consent was obtained from all patients.

Table 1
Patients' data.

Patient number	Gender/age	Number of bevacizumab cycles	Scan dates (days)
1	F 68	6	0, 14, 56
2	M 39	4	0, 11, 52
3	F 51	17	0, 17, 57, 113, 169, 246
4	M 45	12	0, 19, 61, 112, 191
5	F 57	7	0, 54, 110
6	M 34	28[a]	0, 28, 70, 156[b], 245, 312, 379, 466, 555, 655, 708
7	F 60	13	0, 13, 64, 125, 181
8	F 70	7	0, 15, 59
9	M 43	19	0, 15, 56, 113, 169, 225
10	M 51	6	0, 61, 112, 168, 236,
11	F 62	7	0, 14, 56
12	F 74	4	0, 28, 76
13	M 26	3[a]	0, 195[b], 248

All patients were treated with bevacizumab – 10 mg/kg i.v. days 1, 15 of a 28 day cycle.
[a] Patient treated with 5 mg/kg.
[b] Marks beginning of bevacizumab treatment, if not immediately after first scan.

2.2. MR imaging protocol

MR scanning was performed on a 3 Tesla MRI Scanner (GE Signa EXCITE, Milwaukee, WI, USA) using a transmit-receive quadrature head coil. The MR protocol included pre-contrast agent images: spin-echo (SE) T_1 weighted images (WI), (repetition time (TR)/echo time (TE) = 600/8 ms or 540/10 ms), SE T_2 WI (TR/TE = 4500/106 ms), fluid attenuation inversion recovery (FLAIR) (TR/TE/inversion time (TI) = 10,000/117/2500 ms) gradient echo (GE) T_2^* WI (TR/TE/flip angle (FA) = 50/25 ms/20° or 2000/10/ms/90° and 2000/20 ms/90°), and post contrast-agent (gadolinium – DTPA) images: SE T_1 WI (TR/TE = 600/8 ms, 540/10 ms)/spoiled gradient echo (SPGR) (TR/TE/TI/FA = 5.16/1.32/450 ms/12°) and GE T_2^* WI (TR/TE/FA = 50/25 ms/20° or 2000/10 ms/90° and 2000/20 ms/90°). Single voxel MRS was performed using a PRESS sequence (TR/TE = 1500/144 ms) with $10\,mm \times 10\,mm \times 10\,mm$ voxel size performed after contrast agent injection. Several voxels were defined for each patient in the enhancing tumor, non-enhancing tumor, edema-like areas and normal appearing white matter (NAWM) in the hemisphere contra-lateral to the lesion.

2.3. Data analysis

Data analysis included preprocessing and application of in-house modified *k*NN algorithm for tissue classification. Spatial filtering was used for classification and quantification of the enhancing tumor class when compared to manual delineation. Classification results were approved by a senior neuro-radiologist, compared to the manual labeling of the training data set, and validated by MRS. Changes in the volume of the enhancing tumor class were compared to Macdonald's criteria and to 3D manual volumetric measurements. Further sub-classification of the voxels automatically classified as edema-like tissue using the *k*NN algorithm was performed using the EM algorithm on a mixture of Gaussians model.

2.3.1. Preprocessing

B_1 (radiofrequency) field inhomogeneity correction was performed on all images using the N3 algorithm. All MR series from the same subject, within and between scans, were co-registered using rigid-body transformation (by SPM's coregistration module). Series from second and later scans were first coregistered with a representative series from the same scan and then with the representative series of the first scan. Coregistration between scans was performed to facilitate inter-scan visual comparison. MR signal intensity normalization was performed using a multiplicative model, compensating for changes such as those caused by differences in the receiver gain. The single parameter of the model was computed to fix the first peak in a smoothed histogram of the voxel intensities (binned by 1 unit, smoothed using a Gaussian with $\sigma = 16$ bins) to a fixed value. Brain masks were obtained using FMRIB's Brain Extraction Tool.

2.3.2. kNN classification algorithm and modifications

The *k*NN algorithm classifies each voxel by selecting the class (tissue type), which is most popular between similar voxels (in terms of similar signal values in the different contrasts) of the already labeled training set.

Modifications were made for handling differences in imaging protocol. That is, the *k*NN algorithm was performed on several subsets of the available contrasts (e.g. {T_1, T_2 and FLAIR}), which correspond to available training data. Each subset produces a classification based on its partial information. The different classifications were combined into a final classification while considering both their own confidence in their classification (measured by the *k*NN majority vote) and the system's confidence in them (measured by the number of contrasts in the subset). A detailed description of the modifications is provided in the Supplementary Methods.

2.3.3. Training data

Eleven tissue classes were manually labeled in 17 scans from 11 patients: cortical gray matter (GM), deep GM, NAWM, cerebrospinal fluid (CSF), skull, veins (marked on the sagittal sinus), arteries, enhancing tumor, non-enhancing tumor, peri-tumoral edema (defined near the enhancing tumor, <1 cm) and non-peritumoral edema. Normalized intensity histograms of the 11 tissue classes are shown in Fig. S1 of the Supplementary Material.

2.3.4. Spatial filtering

Spatial filtering was applied on the automatically segmented region when quantifying the enhancing tumor class for comparison with manual delineation. This included hole filling in the enhancing tumor binary mask as defined by the *k*NN. Error prone areas were defined as dilated atlas-based CSF region (SPM's ICBM tissue probability atlas in MNI space), deformed into patient's space by the SPM normalization module. Connected components of voxels classified as tumors were dismissed if they had more than 70% overlap with the error prone area.

2.3.5. MR spectroscopy

MRS analysis was performed using Functool software provided by GE (Milwaukee, WI, USA). Choline to creatine ratio (Cho/Cr) and N-acetyl-aspartate to creatine ratio (NAA/Cr) were calculated and the appearance of lipid peaks was assessed. When more than one VOI was defined in the same patient for the same class, a mean value was calculated.

2.4. Validation

The algorithm was performed using leave-one-patient-out (i.e. when classifying a patient's data its own labels are excluded from the training set) and the results were validated against several standards of reference. (a) Manual labeling: the algorithm's classification results were compared to the labels of the training set which was approved by a senior neuro-radiologist. The 11 tissue classes were divided into three groups – healthy tissue (cortical and deep GM, NAWM, CSF, arteries, veins and skull), tumor (enhancing and non-enhancing tumor) and edema-like tissues (peri- and non-peri-tumoral edema). The sensitivity and specificity of the algorithm were calculated based on this partition, which also provided an indirect measure of the accuracy of the training set. (b) MRS: metabolite ratios were calculated from 36 volumes of interest (VOIs), from nine scans of eight patients. MRS VOIs were included only when there was a good overlap with one of the 5 tissue classes: enhancing tumor, non-enhancing tumor, peri-tumoral edema, non-peri-tumoral edema and NAWM, as defined by the *k*NN algorithm. (c) Volumetric measurements: the volume of the enhancing tumor class, defined by the *k*NN algorithm with spatial filter, was compared to the volume of the enhancing tumor defined manually on T_1 post contrast images using Analyze 7.022 (Analyze®; Mayo Clinic, Rochester, MN, USA). Manual delineation of tumor volume was performed in nine patients who had clear borders of the enhancing tumor (total of 33 scans). (d) Independent unsupervised classification: the edema-like area, (i.e. voxels classified as peri- or non-peri-tumoral edema by the *k*NN), was additionally and independently sub-classified by an unsupervised automatic method, expectation–maximization (EM), optimizing a mixture of Gaussians model using the MATLAB implementation of GaussMix into 5 clusters. This classification was performed only on 35 scans of 11 patients who had the full imaging data set of five selected sequences (SE T_1 WI, SE T_2 WI, FLAIR, contrast enhanced SE T_1 WI and SPGR T_1 WI), since this algorithm cannot manage variability in data parameters (i.e. missing data). The results were compared to the *k*NN classification results.

2.5. Therapy response assessment

Progression-free survival (PFS) measurements were calculated, with time-zero for each patient defined as the date of initiation of bevacizumab therapy. Therapy response was assessed based on Macdonald's criteria [2] and longitudinal volumetric changes of the enhancing tumor (based on classification results and manual delineation) and of the edema-like areas.

3. Results

The *k*NN algorithm was applied successfully to all scans, even in the presence of missing data. Fig. 1 shows representative results obtained from three patients. The classification results show spatial continuity (Fig. 1c) although the algorithm does not use any spatial information.

3.1. Validation of the kNN results

3.1.1. Manual labeling of the different tissue classes

The classification of the training set using the leave-one-patient-out method produced sensitivity and specificity of 88% and 90% for the healthy tissue group, 92% and 96% for the tumor groups and 71% and 92% for the edema-like group, respectively.

3.1.2. MRS data

MRS results supported the *k*NN classification of the tissue types, and are presented in Table 2. In some patients several VOIs were defined on the same tissue class and averaged values are given (resulting in 30 locations). The enhancing tumor class was shown to have the highest Cho/Cr values (>1.75 in 4/7 patients), low NAA/Cr ratio (<1.3, in 5/7 patients) and appearance of lipid peaks in 2 patients. The MRS results in the non-enhancing tumor class showed a tumor pattern in two out of three patients (high Cho/Cr and low NAA/Cr ratios), and necrosis pattern in the third patient (appearance of lipids only). The Cho/Cr ratio of the peri-tumoral edema was higher than in the non-peri-tumoral edema, but lower than in the enhancing/non-enhancing tumor (when compared within subjects). This pattern was also obtained in cases where a peri-tumoral edema classified area was distant from the enhancing tumor, while the non-peri-tumoral edema area was in the vicinity of the enhancing tumor. The MRS results in the NAWM were close to normal values in more than half of patients. Four other patients had low or slightly low NAA/Cr values and one patient had high Cho/Cr value (out of 9 patients). Significant correlations were detected between the tissue class and Cho/Cr ratio ($r = 0.483$, $p = 0.007$) and NAA/Cr ratio ($r = -0.56$, $p = 0.001$). These correlations indicate that as the tissue becomes more "malignant", the Cho/Cr ratio rises and the NAA/Cr ratio decreases, as expected.

3.1.3. Volumetric measurement of the enhancing tumor class

The volume of the enhancing tumor class was manually measurable only in about half of the scans (33/59), in which clear borders could be defined. Manual delineations of the enhancing tumor were

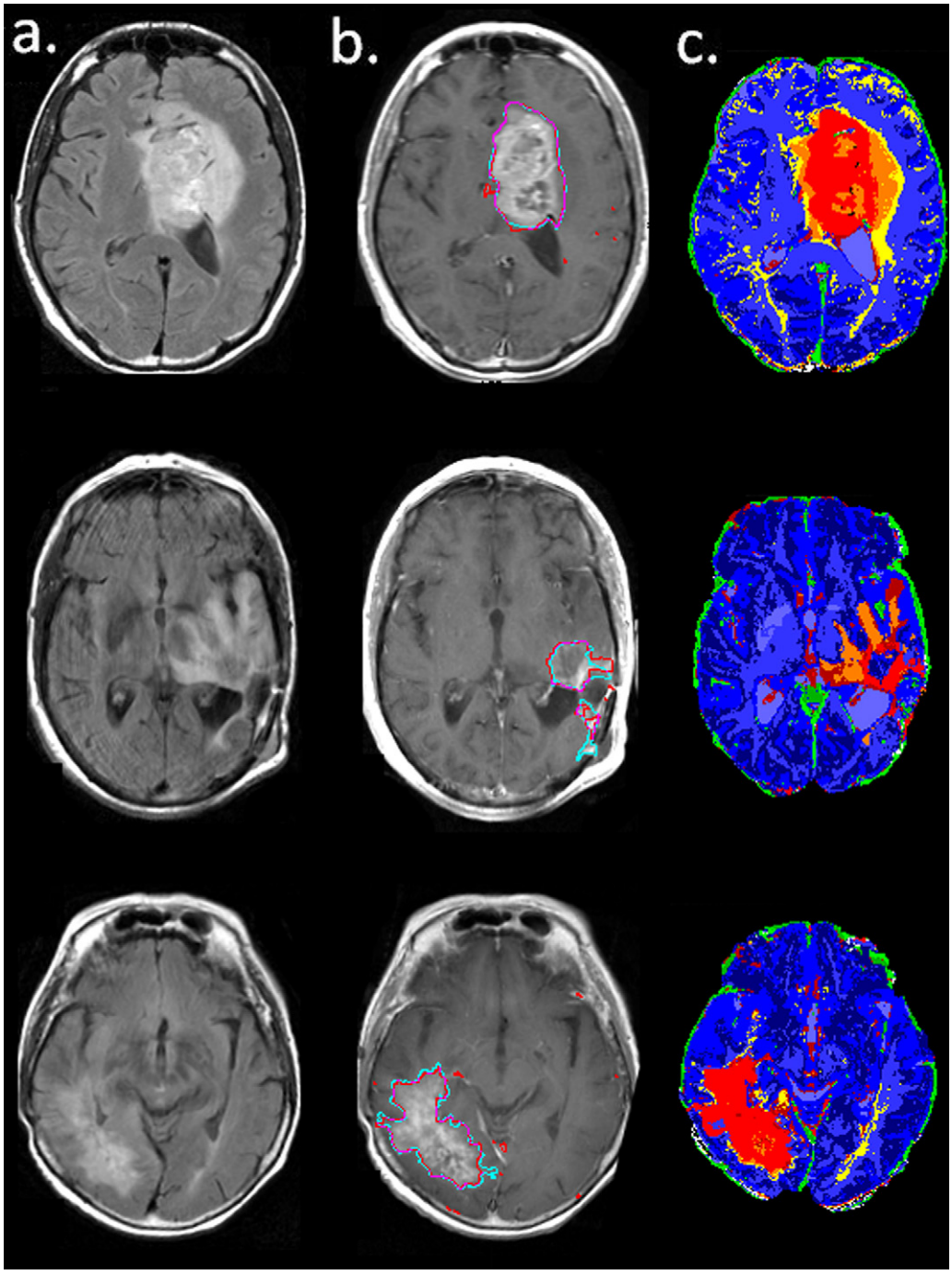

Fig. 1. Representative results obtained from three patients (#6, 11, 12): FLAIR Images – first column; contrast-enhanced SPGR T1 WI overlaid with the *k*NN (red) and manual (turquoise) delineation of the enhancing tumor (violet color represents the area with overlapping signs) – second column; the *k*NN tissue classification results – third column. The 11 classes are marked with: light red ■ – enhancing and dark red ■ – non-enhancing tumor; orange ■ – peri-tumoral and yellow ■ – non-peri-tumoral edema; dark blue ■ – deep GM; blue ■ – cortical GM; light blue ■ WM, and ■ CSF; white □ – skull; dark green ■ – arteries and light green ■ – veins.

approved by a senior neuro-radiologist. Fig. 2 shows a scatter plot of the automatic versus manual volumetric measurements of the enhancing tumor class ($n = 33$, from 9 patients). A strong significant correlation was obtained with $r = 0.96$, $p < 0.0001$ with average overlap of 0.69 (Fig. 2). This high correlation remained even when removing the outlier.

3.1.4. Sub-classification of the edema-like areas

Two classes of edema-like tissue were defined for the supervised (*k*NN) algorithm: peri-tumoral edema (<1 cm from enhancing tumor) and non-peri-tumoral edema. These two classes were combined and re-classified using an unsupervised sub-classification method (EM). The EM defined 5 clusters, 3 of which were related to the peri-tumoral edema class (defined by the *k*NN), and one to the non-peri-tumoral edema class. These two methods provided coherent results, both spatially and quantitatively, showing a significant correlation ($r = 0.91$, $p < 0.00001$). Fig. 4 shows the results of the *k*NN and the EM classification in five patients. As can be seen a good agreement was detected by both methods for the peri-tumoral edema (green) and for the non-peri-tumoral edema (blue).

Table 2
MRS data.

Patient no.	Enhancing tumor			Non-enhancing tumor			Peri-tumoral edema			Non-peri-tumoral edema			White matter		
	Cho/Cr	NAA/Cr	Lip	Cho/Cr	NAA/Cr	Lip	Cho/Cr	NAA/Cr	Lip	Cho/Cr	NAA/Cr	Lip	Cho/Cr	NAA/Cr	Lip
3							1.23	1.25	Non				1.15	1.42	Non
5	2.12	0.4	Yes				1.42	1.2	Non	0.98	0.84	Non	0.78	1.18	Non
6	1.93	0.9	Yes	1.84	1.06	Yes	1.65	1.17	Yes				0.85	1.43	Non
6	1.68	1.24	Non	0	0	Yes	1.70	1.04	Non	1.46	1.11	Non	1.09	1.76	Non
7	2.38	1.5	Non				1.73	1.19	Non	1.6	1.4	Non	1.1	1.67	Non
9	1.4	1.54	Non										1.1	1.65	Non
11				1.52	1.14	Non	1.54	1.12	Yes				1.19	1.5	Non
12	1.42	0.72	Non										0.67	1.1	Non
13	4.63	0.42	Non				3.20	1	Non	1.66	1.88	Non	1.47	2.12	Non

MRS results obtained from the measured tissue classes: enhancing and non-enhancing tumor, edema-like tissue, peri-tumoral edema and white matter, as defined by the algorithm in 36 voxels from 9 scans.

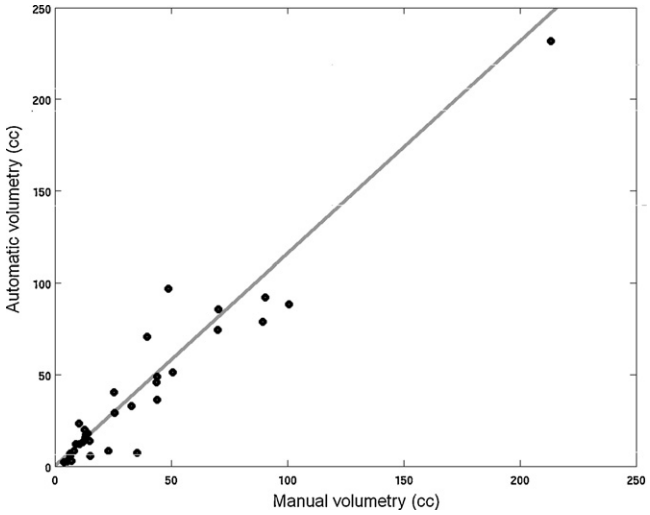

Fig. 2. A scatter plot of automatic versus manual volumetric measurements of the enhancing tumor class ($n = 33$, 9 patients).

3.2. Therapy response assessment

The median PFS of our patients was 141 days, with one patient progression free at 266 days.

Longitudinal assessment of bevacizumab therapy revealed a pattern of early response, as indicated by a reduction in enhancing tumor volume in 12 out of 13 patients. This early response began immediately (first imaging) after bevacizumab administration, and lasted for 2–10 weeks, followed by an increase in the enhancing tumor volume at time of progression.

Fig. 3 shows longitudinal changes for 3 representative cases. The figure shows the volume of the enhancing tumor measured using the *k*NN algorithm (dark gray) compared to the manual definition (light gray) and standard radiologic assessment based on MacDonald's criteria (marked as an upward arrow for progressive disease, downward arrow for partial response and equals sign for stable disease). When calculating the percent volumetric changes obtained from the automatic and manual measurements, only 68% of cases were in agreement with the radiological decision based on Macdonald's criteria.

In order to further assess brain tissue changes following therapy, changes in the volume of sub-classes of the edema-like areas were

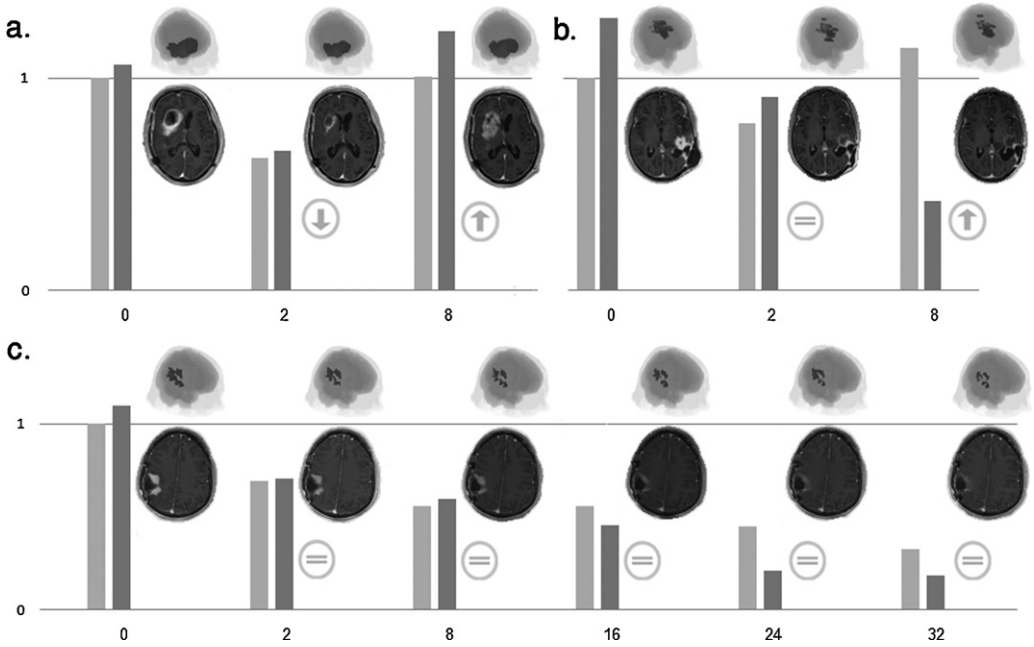

Fig. 3. Longitudinal changes in the volume of the enhancing tumor measured with the *k*NN algorithm (dark gray) and with manual definition (light gray). Radiologic assessment based on Macdonald's criteria – upward arrow for progressive disease, downward arrow for partial response and equals sign for stable disease. A representative slice from an MR image with contrast agent is also shown, along with a 3D view of the tumor, as defined by manual delineation.

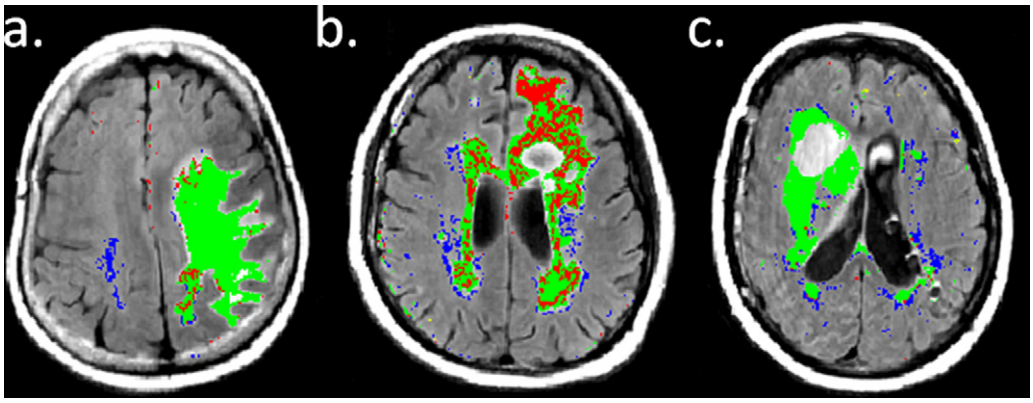

Fig. 4. Classification agreement between *k*NN and EM in three patients (#1, 5, 8). Color coding – agreement on peri-tumoral edema is marked in green and on non-peri-tumoral edema in blue. Disagreement – the *k*NN classified non-peri-tumoral edema is marked in red and as peri-tumoral edema in yellow (this disagreement is almost absent in these examples).

studied. An early response, with reduced volume of both the peri- and non-peri-tumoral edema, was detected in all patients immediately after bevacizumab administration (first or second imaging), with no late increase in volume, except for one patient. In this patient (patient number 4), an increase in peri-tumoral edema was detected 24 weeks after the initiation of therapy. This pattern was shown along with a reduction in the volume of the enhancing tumor class as measured by the *k*NN algorithm (from 29.9 cm^3 at baseline, before initiation of bevacizumab therapy, to 13.7 cm^3 after 24 weeks). Manual measurements of the enhancing tumor could not be performed at week 24 due to the slight and diffused enhancement.

Fig. 5 shows longitudinal results following therapy for one patient. In this patient, a clear border of the enhancing tumor can be detected at baseline (first row), while 24 weeks after bevacizumab therapy (second row) a slight and diffused enhancement with no clear border of a single mass can be seen. The edema-like tissue does not show a clear border on either of these scans preventing accurate manual delineation, yet the automatic methods succeeded in providing such information.

4. Discussion

This study presents the use of automatic algorithms based on multi-modal MR data to improve longitudinal assessment of response in patients with recurrent GB to bevacizumab therapy by monitoring both the enhancing tumor and the edema-like tissue. A classification method was developed, which is robust to variation

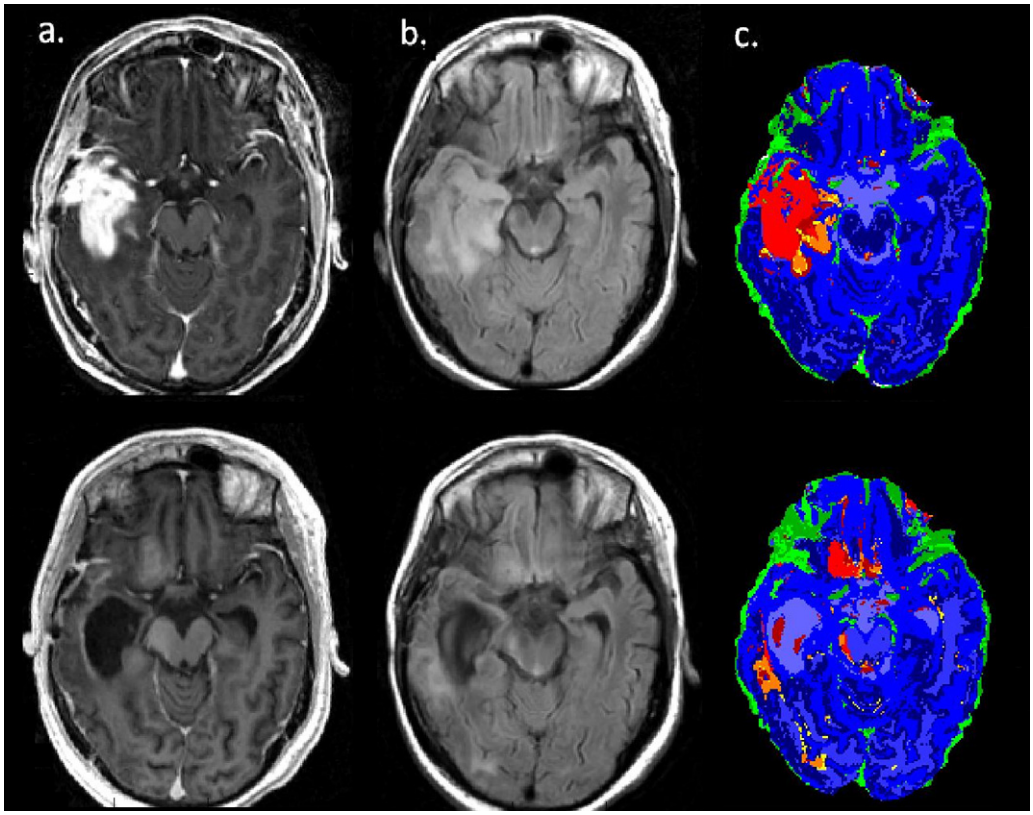

Fig. 5. A representative slice of (a) T_1 post-gadolinium, (b) FLAIR and (c) segmentation results using *k*NN at baseline (first row) and 24 weeks following therapy (second row) in patient number 4.

in the given data and thus is highly applicable to currently available data in multiple institutions. The method successfully classified the various tissues and was validated using several standards of reference. Since the method does not use any spatial information, it can be used independently and complementary to methods based on morphology and location. A significant correlation was demonstrated between the volume of the enhancing tumor class measured using the automatic method and manual measurements, yet not with Macdonald's criteria. Converging results were obtained using supervised and unsupervised classification methods for sub-classification of the edema-like areas demonstrating varying levels of infiltration. In one patient, increased volume was detected in the infiltrative tissue class with no parallel increase in the volume of the enhancing tumor class. This emphasizes the importance of using automatic methods based on multi-modal imaging to provide quantitative information regarding changes in the various tissues, including the edema-like tissue. This may help to better evaluate brain tissue response to therapy, specifically with regard to anti-angiogenic drugs.

4.1. Response to treatment

Twelve out of thirteen patients in this group showed tumor response to bevacizumab treatment during the first 2–10 weeks, as indicated by a reduced enhancing tumor volume, with PFS of ~4.6 months (141 days). These findings are consistent with previous studies reporting median response duration of 3–4 months and demonstrating a reduction in the enhancing tumor tissue and edema-like areas during the first few weeks of therapy [13,14].

4.2. Automatic measurement

A high correlation was detected between automatic and manual volumetric measurements of the enhancing tumor class, yet not with the radiological decision based on Macdonald's criteria. While most clinical trials still employ Macdonald's criteria for evaluating therapy response in high grade gliomas, this method is prone to false diagnosis due to irregularly shaped tumors, changes in slice orientation in follow-up scans, tumor growth in other dimensions, and more. Previous studies have shown substantial inter-radiologist and inter-scan variability in tumor volume assessment [15]. The overlap fraction between the *kNN* and the manual delineation of the enhancing tumor tissue was 0.69, similar to that obtained with other automatic methods [9]. Since clinical decision is largely based on the radiologist's evaluation of changes in tumor volume, longitudinal evaluation, rather than absolute volume measurements, has greater clinical significance. A high correlation was demonstrated between the automatic and manual measurements of the enhancing tumor volume in longitudinal assessment, yet manual segmentations are time consuming, and automatic methods can save valuable expert time while improving diagnostic capability. More importantly, a clear border of the enhancing tumor volume could be manually delineated only in 33/59 scans, while the automatic method successfully classified and measured the enhancing tumor volume in all scans.

The difficulties associated with volumetric tumor measurements have become even more pronounced in the era of anti-angiogenic treatment. Tissue enhancement represents only areas with blood–brain barrier (BBB) disruption, while infiltration of high grade gliomas, specifically those treated with anti-angiogenic therapy, is more diffuse and does not always result in BBB impairment. Anti-angiogenic drugs have been shown to increase the tendency of tumor cells to co-opt existing blood vessels, resulting in a different pattern of invasive non-enhancing tissue [16,17]. Manual delineation of the non-enhancing component of the tumor, which includes peri- and non-peri-tumoral edema changes is even more difficult than measurement of the enhancing tumor, due to unclear borders and overlap with other tissues such as WM changes that may have similar appearance on FLAIR images. In accordance with recent agreement to revise Macdonald's criteria [18,19] and the difficulties of manual delineation, results from this study emphasize the need to include automatic quantitative methods, based on multi-modal data, in routine clinical procedures.

4.3. Edema sub-classification

The training sets for the peri- and non-peri-tumoral edema were defined based on the distance from the enhancing tumor, assuming that infiltration of tumor cells would be larger in proximity to the enhancing tumor. After automatic classification, these two classes did not maintain their spatial dependence in all cases (see Fig. 1). MRS results support this segmentation, and demonstrated a higher malignant pattern in the peri-tumoral edema compared to the non-peri-tumoral edema areas, even far from the enhancing tumor. In order to confirm that the distinction between the two edema sub-classes was inherent, and not dependent on the manual labeling, an unsupervised segmentation method was used (EM), showing high agreement and similar spatial distribution of the peri- and non-peri-tumoral edema. It seems that the peri-tumoral class represents more infiltrative tissue, and indeed, MRS supported a more malignant pattern. Longitudinal changes in the volume of the edema-like tissues demonstrated a different pattern of change that did not match changes in the volume of the enhancing tumor class, and might indicate a pattern of recurrence of a non-enhancing tumor; however additional studies are necessary to validate this hypothesis. Exact localization of the infiltrative tissue may have important clinical value in planning radiation fields or tumor resection.

4.4. Algorithm modification

In this study a modification of the *k*NN algorithm was developed and used for therapy assessment. Differences in acquisition parameters and the absence of several series are inherent problems even in prospective clinical studies due to limitations such as incorrect parameters, patient movements, and time considerations. The modification performed enabled the classification of all scans in spite of missing series, due to selective use of the different data available at different scans of the training set. By creating a site-specific, tissue-specific training data set, the algorithm can overcome the problem of missing series and can be used in multi-center studies. Another popular alternative classification method with inherent robustness to missing values is the Naïve Bayesian network. However the limited power of the latter in describing a complex shape in the high-dimensional attribute space may render it inapplicable to infiltrative tumor cases.

Automatic methods require assessment of the classification results using an accurate standard of reference, which is not always available in human studies. Histopathological samples are an accepted standard of reference; however this requires invasive procedures that cannot routinely be used in therapy assessment. MR spectroscopy is a sensitive, non-invasive method that was shown to correlate with histopathological sampling [20]. In this study, the classification results and the grading of the edema-like tissue obtained by the automatic segmentation methods were confirmed by both MRS and neuro-radiologist assessment. MRS demonstrated elevated Cho/Cr ratios in voxels automatically defined as tumor (enhancing and non-enhancing) or peri-tumoral edema, indicating high proliferation. In these classes, lower NAA/Cr values were also detected with lipids in some of the voxels. The non-enhancing

tumor area showed tumor pattern in two patients and necrosis pattern in a third patient. Indeed, conventional imaging cannot distinguish between these two classes and advanced methods such as diffusion weighted imaging/diffusion tensor imaging and/or perfusion imaging are necessary for this classification [20]. Future studies should incorporate advanced MR methods in the automatic analysis. Voxels of the WM, although taken from the tumor contra lateral hemisphere, were taken from different locations (lobes) within the brain and showed variability in the obtained ratios. All patients had undergone several therapies prior to the use of bevacizumab, including radiation and chemotherapy, and the long term effects of such therapies might also explain the slightly abnormal MRS values in these VOIs.

5. Conclusion

Recent research has shown that radiological evaluation of high-grade glial tumors may be hampered by inaccurate subjective measurement and by limiting treatment response assessment to evaluation of enhancing tissue. In this study both problems were addressed in a unified manner using automated analysis methods based on multiparametric data, classifying the enhancing tumor as well as the edema-like areas. This enabled a more comprehensive analysis of the response to bevacizumab therapy in the tumor and surrounding tissues compared to the standard methods of evaluation. Automatic quantitative methods based on multimodal data improve both efficiency and accuracy of radiologic evaluation, and their role in routine clinical procedure should be developed.

Role of the funding source

The funders had no role in study design, data collection and analysis, decision to publish, or preparation of the manuscript.

Acknowledgment

We thank Moran Artzi for assisting in data collection and helpful discussions and Vicki Myers for editorial assistance.

Appendix A. Supplementary data

Supplementary data associated with this article can be found, in the online version, at http://dx.doi.org/10.1016/j.ejrad.2012.09.001.

References

[1] Prados M, Cloughesy T, Samant M, et al. Response as a predictor of survival in patients with recurrent glioblastoma treated with bevacizumab. Neuro-Oncology 2010;13:143–51.
[2] Macdonald DR, Cascino TL, Schold SC, Cairncross JG. Response criteria for phase II studies of supratentorial malignant glioma. Journal of Clinical Oncology: Official Journal of the American Society of Clinical Oncology 1990;8:1277–80.
[3] Batchelor TT, Sorensen AG, di Tomaso E, et al. AZD2171, a pan-VEGF receptor tyrosine kinase inhibitor, normalizes tumor vasculature and alleviates edema in glioblastoma patients. Cancer Cell 2007;11:83–95.
[4] Sorensen A, Batchelor T, Wen P, Zhang W, Jain R. Response criteria for glioma. Nature Clinical Practice Oncology 2008;5:634–44.
[5] Akselrod-ballin A, Galun M, Gomori MJ, et al. An integrated segmentation and classification approach applied to multiple sclerosis analysis. In: Proceedings of the 2006 IEEE Computer Society Conference on Computer Vision and Pattern Recognition. 2006. p. 1122–9.
[6] Karayiannis NB, Pai PI. Segmentation of magnetic resonance images using fuzzy algorithms for learning vector quantization. IEEE Transactions on Medical Imaging 1999;18:172–80.
[7] Vijayakumar C, Damayanti G, Pant R, Sreedhar CM. Segmentation and grading of brain tumors on apparent diffusion coefficient images using self-organizing maps. Computerized Medical Imaging and Graphics: The official Journal of the Computerized Medical Imaging Society 2007;31:473–84.
[8] Lee MC, Nelson SJ. Supervised pattern recognition for the prediction of contrast-enhancement appearance in brain tumors from multivariate magnetic resonance imaging and spectroscopy. Artificial Intelligence in Medicine 2008;43:61–74.
[9] Corso J, Sharon E, Dube S. Efficient multilevel brain tumor segmentation with integrated bayesian model classification. Medical Imaging 2008;27:629–40.
[10] Zacharaki EI, Wang S, Chawla S, et al. Classification of brain tumor type and grade using MRI texture and shape in a machine learning scheme. Magnetic Resonance in Medicine 2009;62:1609–18.
[11] Verma R, Zacharaki EI, Ou Y, et al. Multiparametric tissue characterization of brain neoplasms and their recurrence using pattern classification of MR images. Academic Radiology 2008;15:966–77.
[12] Dudani S. The distance-weighted *k*-nearest-neighbor rule. IEEE Transactions on Systems, Man, and Cybernetics 1976;SMC-6:325–7.
[13] Ananthnarayan S, Bahng J, Roring J, et al. Time course of imaging changes of GBM during extended bevacizumab treatment. Journal of Neuro-Oncology 2008;88:339–47.
[14] Khasraw M, Lassman AB. Advances in the treatment of malignant gliomas. Current Oncology Reports 2010;12:26–33.
[15] Prastawa M, Bullitt E. A brain tumor segmentation framework based on outlier detection. Medical Image Analysis 2004;8:275–83.
[16] Bergers G, Hanahan D. Modes of resistance to anti-angiogenic therapy. Nature Reviews Cancer 2008;8:592–603.
[17] Pāez-Ribes M, Allen E, Hudock J. Antiangiogenic therapy elicits malignant progression of tumors to increased local invasion and distant metastasis. Cancer Cell 2009;15:220–31.
[18] Pope WB, Young JR, Ellingson BM. Advances in MRI assessment of gliomas and response to anti-VEGF therapy. Current Neurology and Neuroscience Reports 2011;11:336–44.
[19] Wen PY, Macdonald DR, Reardon DA, et al. Updated response assessment criteria for high-grade gliomas: response assessment in neuro-oncology working group. Journal of Clinical Oncology: Official Journal of the American Society of Clinical Oncology 2010;28:1963–72.
[20] Law M. Advanced imaging techniques in brain tumors. Cancer Imaging 2009;9:S4–9.